Study of Matter Density Distributions, Elastic Electron Scattering form Factors and Reaction Cross Sections of ^{8}He And ^{17}B Exotic Nuclei

Adel K. Hamoudi, Gaith N. Flaiyh, Ahmed N. Abdullah*
Department of Physics, College of Science, University of Baghdad, Baghdad, Iraq.

Abstract

The ground state densities of unstable neutron-rich ^{8}He and ^{17}B exotic nuclei are studied via the framework of the two-frequency shell model (TFSM) and the binary cluster model (BCM). In TFSM, the single particle harmonic oscillator wave functions are used with two different oscillator size parameters β_c and β_v where the former is for the core (inner) orbits and the latter is for the valence (halo) orbits. In BCM, the internal densities of the clusters are described by single particle Gaussian wave functions. Shell model calculations for the two valence neutrons in ^{8}He and ^{17}B are performed via the computer code OXBASH. The long tail performance is clearly noticed in the calculated neutron and matter density distributions of these nuclei. The structure of the two valence neutrons in ^{8}He and ^{17}B is found to be a mixed configurations with dominant $(1p_{1/2})^2$ and $(2s_{1/2})^2$, respectively. Elastic electron scattering proton form factors for ^{8}He and ^{17}B are studied using the plane wave born approximation (PWBA). It is found that the major difference between the calculated form factors of unstable nuclei [^{8}He, ^{17}B] and those of stable nuclei [^{4}He, ^{10}B] is the difference in the center of mass correction which depends on the mass number and the size parameter β (which is assumed in this case as the average of β_c and β_v). The reaction cross sections for ^{8}He and ^{17}B are studied by means of the Glauber model with an optical limit approximation using the ground state densities of the projectile and target, where these densities are described by single Gaussian functions. The calculated reaction cross sections of ^{8}He and ^{17}B at high energy are in good agreement with the experimental data. The analysis of the present study supports the halo structure of these nuclei.

Keywords: neutron-rich exotic nuclei; shell model calculations; elastic electron scattering form factor; density distributions; root mean square radii of halo nuclei
PACS number(s): 21.10.Gv, 25.30.Bf, 21.10.ft

دراسة توزيعات الكثافة و عوامل التشكل للاستطارة الالكترونية المرنة و المقاطع العرضية للتفاعل للنوى الغريبة ^{8}He و ^{17}B

عادل خلف حمودي، غيث نعمة فليح، أحمد نجم عبدالله*
قسم الفيزياء، كلية العلوم، جامعة بغداد، بغداد، العراق

الخلاصة

تم حساب توزيعات الكثافة للنوى الغريبة غير المستقرة والغنية بالنيوترونات ^{8}He و ^{17}B باستخدام أنموذج القشرة ذو الترددين (TFSM) والانموذج العنقودي الثنائي (BCM). في انموذج القشرة ذو الترددين استُخدمت الدوال الموجية للجسيمة المفردة لجهد المتذبذب التوافقي مع قيمتين مختلفتين للثابت التوافقي احدهما (β_c)

*Email: Ahmednajim1979@yahoo.com

للقلب و الاخرى (β_v) للنيوكليونات الفعالة (الموجودة خارج القلب النووي) . في الانموذج العنقودي الثنائي تم وصف الكثافة الداخلية للعنقودين باستخدام دالة گاوس للجسيمة المفردة. الامتداد الطويل ظهر بوضوح في توزيعات الكثافة النيوترونية والكتلية لهذه النوى. اوضحت هذه الدراسة بان النيوكليونات الفعالة للنوى ^{8}He و ^{17}B تتركب من حالات ممتزجة وبهيمنة التشكيلات $(1p_{1/2})^2$ و $(2s_{1/2})^2$ على التوالي. لقد تم تحليل نتائج عوامل التشكل المرنة لبروتونات هذه النوى بواسطة تقريب بورن للموجة المستوية. وجد ان الاختلاف بين عوامل التشكل للنوى الغريبة [^{17}B, ^{8}He] ونظيرتها المستقرة [^{10}B , ^{4}He] يعود الى التباين في عامل تصحيح مركز الكتلة والذي يعتمد على العدد الكتلي وثابت المتذبذب التوافقي (β).

المقاطع العرضية للتفاعل لهذه النوى عند الطاقات العالية تم دراستها باستخدام نموذج گلوبر باستخدام توزيع الكثافة للحالة الارضية للنواة القذيفة والهدف، حيث ان هذه الكثافات توصف بواسطة دوال گاوس للجسيمة المنفردة. ان حسابات المقاطع العرضية للتفاعل لهذه النوى تتفق بشكل جيد مع القيم العملية.

1. Introduction

The development of radioactive nuclear beams in the mid-eighties enabled physicists to study nuclei far from stability [1, 2]. This led to the discovery of neutron halo nuclei. Halo nuclei are weakly bound and spatially extended systems, they are threshold phenomenon, as the binding energy of the last nucleon(s) becomes small, the nucleon(s) becomes in the proximity of the particle continuum, the tail of the wave function extends more and more outward the central nuclear confining potential well which leads to the formation of a diffuse nuclear cloud due to quantum-mechanical penetration (the so-called nuclear halo); in turn such large diffusivity causes unusual spatial properties of the nucleon density distribution, leading to nuclear sizes deviating substantially from the $R = R_0 A^{1/3}$ rule. Halo nuclei are fragile and oversized, they are expected to appear along the drip curves, their structure are imagined to be composed of a tightly bound core surrounded by one or few loosely nucleons (two-nucleon halo is called Borromean [3], where none of the binary subsystems of the core plus two-nucleons are found in bound structure). Halo nucleon(s) prefers to occupy orbits with low orbital quantum numbers, in s- or p-orbital; to lower the confining effect coming from Coulomb and centrifugal barrier which push or suppress the tail of the radial wave function toward core; leading to non-halo behavior. Halo nuclei are so short lived that they cannot be used as targets at rest. Therefore, experiments have been done in inverse kinematics (i.e., the role of target and projectile are exchanged) with a beam of exotic nuclei incident on a stable target at radioactive ion beam (RIB) facilities [4].

Electron scattering from nuclei is a powerful to investigate the electromagnetic structure in stable nuclei. This is because of the relatively weak interaction of electron with nucleus which is done through the well-known electromagnetic force [5]. Electron scattering from exotic nuclei is not presently available; the technical proposal for the construction of electron-ion collider at GSI/Germany [6] and RIKEN/Japan facility [7] will be a great opportunity to study the electromagnetic structure of these exotic nuclei in the near future.

As it follows from the analyses of the cross sections [8,9], ^{8}He nucleus exhibits significant halo structures. The charge and matter distributions of He-isotopes [10-12] were tested in analyses of total reaction cross sections of the proton scattering on exotic nuclei using different phenomenological and theoretical methods.

From a theoretical point of view [13], ^{17}B was predicted to have a two-neutron halo with the core ^{15}B plus two valence neutrons. Suzuki et al. [14] studied the interaction cross section for ^{17}B on a carbon target at 880 A MeV. The result for σI was 1118±22 mb. They also studied the root mean square (rms) matter radii of ^{17}B using the Glauber-type calculation based on the optical limit approximation and a few-body reaction model. Their results for these two different methods were 2.90 ± 0.06 and 2.99 ± 0.09 fm, respectively.

The total nuclear reaction cross section (σ_{tot}) is one of the most important physical quantities characterizing the properties of nuclear reaction [15]. It is very useful for extracting fundamental information about the nuclear size and the density distributions of neutrons and protons in nucleus. In particular, the neutron halo has been found by measuring the total reaction cross section induced by radioactive nuclear beams [1, 16]. The definition of the reaction cross section (σ_R) and the interaction cross section (σ_I) are [17]: $\sigma_R = \sigma_{tot} - \sigma_{ela}$ and $\sigma_I = \sigma_R - \sigma_{inela}$, where σ_{ela} and σ_{inela} are the elastic

and inelastic scattering cross sections, respectively. At high energy (above several hundred MeV/nucleon), it is known that σ_R is approximated by σ_I ($\sigma_R \approx \sigma_I$) because the contribution of the inelastic scattering is low [18, 19]

One of the widely used models for analyzing the interaction and the reaction cross sections of nucleus-nucleus scattering is the Glauber model [20]. In ref. [21], a simple Glauber model was used to connect the density distributions and cross sections. Although this model is simple, it shows reasonable results of many cases for the reactions of the stable and exotic nuclei. A modified microscopic Glauber theory was used to investigate the reaction projectile-target collisions at low and intermediate energies. The calculated reaction cross sections [20, 22] at intermediate energies were in good agreement with the experimental data.

In the present study, we analyze the ground state densities, elastic electron scattering proton form factors and reaction cross sections of unstable neutron-rich ^{8}He [^{17}B] exotic nucleus. The structure of the two valence neutrons in ^{8}He [^{17}B] is investigated and found to be a mixed configurations with dominant $(1p_{1/2})^2$ [$(2s_{1/2})^2$] in ^{8}He [^{17}B]. Elastic electron scattering proton form factors for ^{8}He [^{17}B] is studied through combining the proton density distribution, obtained by the TFSM, with the PWBA. The difference between the calculated form factors of unstable exotic nucleus ^{8}He [^{17}B] and that of stable nucleus ^{4}He [^{10}B] is analyzed and attributed to the difference in the center of mass correction which depends on the mass number and the size parameter β (which is assumed in this case as the average of β_c and β_v). The reaction cross sections for ^{8}He [^{17}B] is examined by means of the Glauber model with an optical limit approximation using the ground state densities of the projectile and target. The calculated reaction cross sections at high energies are in good agreement with the data. The analysis of the present study suggests the halo structure of these exotic nuclei.

2. Theory

The one-body operator of the longitudinal transition density for point protons (with isospin $t_z = 1/2$) or neutrons ($t_z = -1/2$) is given by

$$\hat{\rho}^L_{\Delta J,t_z} = \sum_{k=1}^{A} e(t_z)\frac{\delta(r-r_k)}{r_k^2} Y_{\Delta J,M_{\Delta J}}(\Omega_{r_k}), \quad (1)$$

with

$$e(t_z) = \frac{1+2t_z(k)}{2}.$$

In Eq. (1), the superscript (L) in the operator $\hat{\rho}^L_{\Delta J,t_z}$ stands for a longitudinal operator, $Y_{\Delta J,M_{\Delta J}}(\Omega_{r_k})$ and $\delta(\vec{r}-\vec{r}_k)$ are the spherical harmonic and Dirac delta functions, respectively. The multipolarity ΔJ of the transition is restricted by the following angular momentum and parity selection rules:

$$\left|J_i \_ J_f\right| \le \Delta J \le J_i + J_f$$

and

$\pi_i \pi_f = (-1)^{\Delta J}$ (for Coulomb transitions).

The reduced matrix element of Eq. (1) is expressed as

$$\left\langle J_f \left\| \hat{\rho}^L_{\Delta J,t_z}(\vec{r}) \right\| J_i \right\rangle = \frac{1}{\sqrt{4\pi(2J_i+1)}} \sum_{ab} OBDM(J_f, J_i, \Delta J, a, b, t_z) \left\langle j_a \left\| Y_{\Delta J} \right\| j_b \right\rangle R_{n_a l_a}(r) R_{n_b l_b}(r), \quad (2)$$

where a and b label single-particle states for the considered shell model space, i.e. $|a\rangle = |n_a l_a\rangle |j_a m_a\rangle$ and $|b\rangle = |n_b l_b\rangle |j_b m_b\rangle$, the states $|J_i\rangle$ and $|J_f\rangle$ are characterized by the model space wave functions, $R_{n_p l_p}(r)$ is the radial part of the harmonic oscillator wave function,

$\left\langle j_a \| Y_{\Delta J} \| j_b \right\rangle$ is the reduced matrix element of the spherical harmonic, $OBDM(J_f, J_i, \Delta J, a, b, t_z)$ is the proton ($t_z = 1/2$) or neutron ($t_z = -1/2$) one body density matrix element given by the second quantization as

$$OBDM(J_f, J_i, \Delta J, a, b, t_z) = \frac{\left\langle J_f \left\| \left[a^+_{a,t_z} \otimes \tilde{a}_{b,t_z} \right]^{\Delta J} \right\| J_i \right\rangle}{\sqrt{2\Delta J + 1}}. \tag{3}$$

As the model space wave functions have good isospin, it is appropriate to evaluate the *OBDM* elements by means of isospin-reduced matrix elements. The relation between these triply reduced *OBDM* and the proton or neutron *OBDM* of Eq. (2) is given by [23]

$$\begin{aligned} OBDM(t_z) = (-1)^{T_f - T_z} \sqrt{2} \begin{pmatrix} T_f & 0 & T_i \\ -T_z & 0 & T_z \end{pmatrix} OBDM(\Delta T = 0)/2 \\ + 2t_z (-1)^{T_f - T_z} \sqrt{6} \begin{pmatrix} T_f & 1 & T_i \\ -T_z & 0 & T_z \end{pmatrix} OBDM(\Delta T = 1)/2 \end{aligned} \tag{4}$$

where the triply reduced $OBDM(\Delta T)$ elements are given in terms of the second quantization as

$$OBDM(i, f, \Delta J, \alpha, \beta, \Delta T) = \frac{\left\langle \Gamma_f \left\| \left[a^+_\alpha \otimes \tilde{a}_\beta \right]^{\Delta J, \Delta T} \right\| \Gamma_i \right\rangle}{\sqrt{2\Delta J + 1}\sqrt{2\Delta T + 1}} \tag{5}$$

Here, Greek symbols are utilized to indicate quantum numbers in coordinate space and isospace (i.e., $\alpha \equiv at_a$, $\beta \equiv bt_b$, $\Gamma_i \equiv J_i T_i$ and $\Gamma_f \equiv J_f T_f$).

The $OBDM(\Delta T)$ elements contain all of the information about transitions of given multipolarities which are embedded in the model space wave functions. To obtain these *OBDM* elements, we perform shell model calculations by OXBASH code [24] using realistic effective interactions.

For the ground state density distribution, we have $n_a = n_b$, $l_a = l_b$, $j_a = j_b$, $J_i = J_f$ and $\Delta J = 0$, then Eq. (2) becomes as

$$\begin{aligned} \rho_{t_z}(r) &\equiv \left\langle J_i \left\| \hat{\rho}^L_{\Delta J = 0, t_z}(\vec{r}) \right\| J_i \right\rangle \\ &= \frac{1}{\sqrt{4\pi(2J_i + 1)}} \sum_{ab} OBDM(J_i, J_i, 0, a, b, t_z) \left\langle j_a \| Y_0 \| j_b \right\rangle R_{n_a l_a}(r) R_{n_b l_b}(r), \end{aligned} \tag{6}$$

where

$$\left\langle j_a \| Y_0 \| j_b \right\rangle = \left\langle j_a \left\| \frac{1}{\sqrt{4\pi}} \right\| j_b \right\rangle = \frac{1}{\sqrt{4\pi}} \left\langle j_a \| 1 \| j_b \right\rangle = \frac{1}{\sqrt{4\pi}} \sqrt{2j_a + 1}\, \delta_{j_a j_b}. \tag{7}$$

The average occupation number in each orbit n_{a,t_z} is given by

$$n_{a,t_z} = \sqrt{\frac{2J_a + 1}{2J_i + 1}}\, OBDM(J_i, J_i, 0, a, a, t_z). \tag{8}$$

As the exotic halo nuclei are oversized and easily broken systems consisting of a compact core plus a number of outer nucleons loosely bound and spatially extended far from the core, it is suitable to

separate the ground state matter density distribution $\rho_{t_z,m}(r)$ into two parts. The first part is connected to the core nucleons $\rho_{t_z,c}(r)$ while the second is connected to the valence (halo) nucleons

$\rho_{t_z,v}(r)$, (for simplicity, the subscript t_z in these densities will be dropped), i.e.

$$\rho_m(r) = \rho_c(r) + \rho_v(r). \quad (9)$$

Two approaches are utilized for calculating the ground state densities of exotic nuclei, these are the two frequency shell model (TFSM) and the binary cluster model (BCM).

In TFSM [25, 26], the harmonic oscillator wave functions (HO) are used with two different oscillator size parameters β_c (for core nucleons) and β_v (for halo nucleons). This approach permits to work freely on each part by changing $\beta_{c(v)}$ till obtaining a fit with observed data. Furthermore, the matter density of Eq. (9) may also be expressed as

$$\rho_m(r) = \rho^p(r) + \rho^n(r), \quad (10)$$

where $\rho^p(r)$ and $\rho^n(r)$ are the ground state proton and neutron densities of halo nuclei expressed as

$$\rho^p(r) = \rho_c^p(r) + \rho_v^p(r) \quad (11)$$

and

$$\rho^n(r) = \rho_c^n(r) + \rho_v^n(r). \quad (12)$$

The normalization conditions for the ground state densities given in Eqs. (9-12) are

$$g = 4\pi \int_0^\infty \rho_g(r) r^2 dr, \quad (13)$$

and the corresponding rms radii are

$$< r^2 >_g^{1/2} = \frac{4\pi}{g} \int_0^\infty \rho_g(r) r^4 dr, \quad (14)$$

where $\rho_g(r)$ corresponds to the one of the densities [$\rho_m(r)$, $\rho_c(r)$, $\rho_v(r)$, $\rho^p(r)$, $\rho^n(r)$] and g corresponds to the number of nucleons in each case.

Next we use the plane wave Born approximation (PWBA) to study the elastic electron scattering form factors from considered nuclei. In the PWBA, the incident and scattered electron waves are represented by plane waves. The elastic proton form factor is simply given by the Fourier-Bessel transform of the ground state proton density distribution obtained by TFSM, i.e.

$$F(q) = \frac{4\pi}{Z} \int_0^\infty \rho^p(r) j_0(qr) r^2 dr, \quad (15)$$

where $j_0(qr)$ is the spherical Bessel function of order zero and *q* is the momentum transfer from the incident electron to the target nucleus. Inclusion the corrections of the finite nucleon size $F_{fs}(q) = \exp(-0.43q^2/4)$ and the center of mass $F_{cm}(q) = \exp(b^2q^2/4A)$ in the calculations needs multiplying the form factor of Eq. (15) by these corrections.

In BCM [27], the exotic nuclei are considered as composite projectiles of mass A_p and described, in figure-1, as core and valence clusters, of masses A_c and A_v bounded with a state of relative motion. It is assumed that $A_c \geq A_v$. For simplicity, the internal densities of clusters are described by single Gaussian functions with ranges α_c and α_v,

$$\rho_c(r) = A_c g^{(3)}(\alpha_c, r),$$
$$\rho_v(r) = A_v g^{(3)}(\alpha_v, r), \quad (16)$$

where $g^{(3)}$ is the normalized 3-dimensional Gaussian function

$$g^{(3)}(\alpha_{c(v)}, r) = \frac{1}{\pi^{3/2}\alpha_{c(v)}^3}\exp(-r^2/\alpha_{c(v)}^2), \ \int g^{(3)}(\alpha_{c(v)}, r)d\vec{r} = 1, \ <r^2>_{c(v)} = 3\alpha_{c(v)}^2/2. \quad (17)$$

Upon convoluting the intrinsic cluster densities with their center of mass (c.m.) motions about the c.m. of the projectile, the composite projectile density is given by [27]

$$\rho_P(r) = A_c g^{(3)}(\hat{\alpha}_c, r) + A_v g^{(3)}(\hat{\alpha}_v, r) \quad (18)$$

with range parameters

$$\hat{\alpha}_v^2 = \alpha_v^2 + \left(\frac{A_c\alpha}{A_v + A_c}\right)^2, \quad \hat{\alpha}_c^2 = \alpha_c^2 + \left(\frac{A_v\alpha}{A_v + A_c}\right)^2. \quad (19)$$

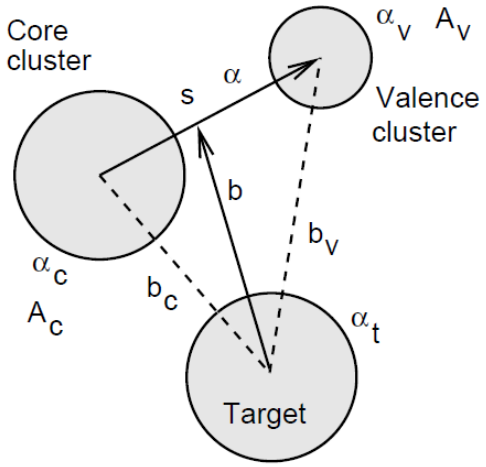

Figure.1- the two-cluster projectile and target coordinates.

The mean squared radius of the composite projectile $<r^2>_P$ satisfies

$$A_P <r^2>_P = A_c <r^2>_c + A_v <r^2>_v + \frac{A_v A_c}{A_P} <r^2> = \frac{3}{2}\left(A_v\hat{\alpha}_v^2 + A_c\hat{\alpha}_c^2\right) \quad (20)$$

This approach provides a projectile density with distinct components due to the valence and core clusters. Such simple two component forms can be employed for calculating the density distributions of light exotic nuclei and also employed as input to optical limit calculations of reaction cross sections. However, a particular projectile single particle density, described by a given (A_c,A_v) mass split and choice of the two component ranges ($\hat{\alpha}_c, \hat{\alpha}_v$), does not define the underling structure of the projectile. If one of the original clusters is point like, for example $\alpha_v = 0$, then fixing $\hat{\alpha}_v$ and $\hat{\alpha}_c$ uniquely determines α and hence α_c.

The reaction cross sections for considered exotic nuclei are studied by Glauber model [27], where the internal motions of particles within the projectile (P) and target (T) are assumed slow compared to the relative motion of centers of mass of the projectile and target. The reaction cross section for a projectile incident upon a target is given by [28]

$$\sigma_R = 2\pi \int_0^{\infty} b[1-T(b)]db\left(1-\frac{B_c}{E_{cm}}\right), \tag{21}$$

where B_c is Coulomb barrier, E_{cm} is the kinetic energy in the center of mass system and $T(b)$ is the transparency function at impact parameter b. A straightforward calculation of $T(b)$ is very complicated. One of the simplest methods to calculate $T(b)$ is the Optical limit (OL) approximation. In this approximation, which ignores any correlations between particles in the projectile or target, $T(b)$ is written as the squared modulus of the elastic $S-$matrix for the projectile-target system.

$$T(b) = \left|S_{el}^{OL}(b)\right|^2, \tag{22}$$

where

$$S_{el}^{OL}(b) = \exp\left[i\mathrm{O}_{PT}(b)\right], \tag{23}$$

and

$$\mathrm{O}_{PT}(b) = \int_{-\infty}^{\infty} dR_3 \int d\vec{r}_1 \int d\vec{r}_2 \rho_P(r_1)\rho_T(r_2) f_{NN}\left(\left|\vec{R}+\vec{r}_1-\vec{r}_2\right|\right) \tag{24}$$

is the overlap of the projectile and target ground state densities (ρ_P and ρ_T, respectively) with an effective nucleon-nucleon (NN) amplitude [$f_{NN}(r)$] integrated along the assumed straight curve path of the projectile's center of mass at impact parameter b. For zero-range NN amplitude and isospin $T=0$ target, $f_{NN}(r)$ has the form [29]

$$f_{NN}(r) = (i\bar{\sigma}_{NN}/2)\,\delta(r) \tag{25}$$

where $\bar{\sigma}_{NN}$ is the average of the free neutron-neutron (nn) and neutron-proton (np) total cross section at the energy of interest. An explicit form for $\bar{\sigma}_{NN}$ is given in ref. [30]. Expressing the projectile-target separation in cylindrical coordinates $\vec{R} = (\vec{b}, R_3)$, where $z=3$ is the axis chosen along the incident beam direction, then [with the help of Eqs. (24) and (25)] Eq. (23) gives

$$S_{el}^{OL}(b) = \exp\left[-\frac{\bar{\sigma}_{NN}}{2}\int d\vec{r}_1 \int d\vec{r}_2 \rho_P^z(r_1)\rho_T^z(r_2)\delta(\left|\vec{b}+\vec{r}_1-\vec{r}_2\right|)\right]. \tag{26}$$

Integrating over the coordinates r_2 then replacing r_1 by s, we obtain

$$S_{el}^{OL}(b) = \exp\left[-\frac{\bar{\sigma}_{NN}}{2}\int d\vec{s}\,\rho_P^z(s)\rho_T^z(\left|\vec{b}+\vec{s}\right|)\right], \tag{27}$$

where $\rho_{P(T)}^z(s)$ is the z-direction integrated nucleon density distribution expressed as

$$\rho_{P(T)}^z(s) = \int_{-\infty}^{\infty} \rho_{P(T)}\left(\sqrt{s^2+z^2}\right)dz. \tag{28}$$

It is obvious from Eq. (27) that the calculations of $S_{el}^{OL}(b)$ requires only the projectile and target ground state densities. For simplicity, both densities are described by single Gaussian functions with range parameters α_P and α_T, respectively.

Results and discussion

The ground state proton, neutron and matter densities of the ^{8}He ($S_{2n}=2.14$ MeV, $\tau_{1/2}=1.19$ ms) [31, 32] and ^{17}B ($S_{2n}=1.34$ MeV, $\tau_{1/2}=5.08$ ms) [31, 32] exotic nuclei are studied by means of the TFSM [25] and BCM [27].

In TFSM, the calculations are based on using different model spaces for the core and valence (halo) neutrons. The single particle harmonic oscillator wave functions are employed with two different size parameters β_c and β_v. The nucleus ^{8}He ($J^{\pi},T=0^{+},2$) is formed by coupling the core ^{6}He ($J^{\pi},T=0^{+},1$) with the valence two neutrons ($J^{\pi},T=0^{+},1$). The nucleus ^{17}B ($J^{\pi},T=3/2^{-},7/2$) is formed by coupling the core ^{15}B ($J^{\pi},T=3/2^{-},5/2$) with the valence two neutrons ($J^{\pi},T=0^{+},1$). The configurations $(1s_{1/2})^4$, $(1p_{3/2})^2$ and $(1s_{1/2})^4$, $(1p_{3/2})^7$, $(1p_{1/2})^2$, $(1d_{5/2})^2$ are assumed for core nuclei ^{6}He and ^{15}B, respectively. Three different configurations are considered for the description of the two valence neutrons in ^{8}He and ^{17}B. For ^{8}He, the two valence neutrons are assumed to be in the pure $1p_{1/2}$, the pure $1d_{5/2}$ and the model space of Zuker-Buck- Mcgrory (ZBM), which includes the orbitals $1p_{1/2}$, $1d_{5/2}$ and $2s_{1/2}$,while for ^{17}B, they are assumed to be in the pure $1d_{3/2}$, the pure $2s_{1/2}$ and the model space of HASP ($1d_{3/2}$, $2s_{1/2}$, $2p_{3/2}$ and $1f_{7/2}$ orbits).

To obtain the OBDM elements for the two valence neutrons occupying the model space ZBM (in ^{8}He) [HASP (in ^{17}B)], shell model calculations are performed via the computer code OXBASH [24] using the realistic interaction of REWIL [33] [HASP [34]]. The ground state occupation numbers for the two valence neutrons in ^{8}He are 1.605 for $(1p_{1/2})^2$, 0.345 for $(1d_{5/2})^2$ and 0.050 for $(2s_{1/2})^2$ and in ^{17}B are 0.284 for $(1d_{3/2})^2$, 1.200 for $(2s_{1/2})^2$, 0.126 for $(2p_{3/2})^2$ and 0.390 for $(1f_{7/2})^2$. These occupation numbers indicate that the structure of the two valence neutrons in ^{8}He [^{17}B] is mixed configurations with dominant $(1p_{1/2})^2$ [$(2s_{1/2})^2$]. As the halo nucleons prefer to occupy orbits with low orbital quantum numbers (such as the s or p-orbital), these occupation numbers supports the halo structure of these nuclei.

Table-1 displays the values of the harmonic oscillator size parameter β_c and β_v utilized in the present calculations for ^{8}He and ^{17}B exotic nuclei. It is clear from this table that the calculated rms matter radii for core [^{6}He, ^{15}B] and exotic nuclei [^{8}He, ^{17}B] using these values of β_c and β_v are in very good agreement with those of experimental results.

Table 1- Parameters for β_c and β_v utilized in the TFSM of the present study together with the calculated and experimental rms radii of ^{8}He and ^{17}B exotic nuclei.

Exotic nuclei	Core nuclei	β_c (fm)	β_v (fm)	rms matter radii for core nuclei $< r^2 >_{core}^{1/2}$ (fm)		rms matter radii for exotic nuclei $< r^2 >_{exotic}^{1/2}$ (fm)	
				Calculated results	Experimental results	Calculated results	Experimental results
^{8}He	^{6}He	1.699	2.237	2.30	2.30±0.07 [35]	2.70	2.70±0.03 [2]
^{17}B	^{15}B	1.485	3.134	2.28	2.28±0.02 [36]	2.99	2.99±0.09 [37]

In BCM [27], the exotic nucleus is considered as a composite projectile consisting of core and valence clusters bound with a state of relative motion figure-1. The internal densities of the clusters, given by Eq. (16), are described by single particle Gaussian wave functions. The composite projectile densities of ^{8}He and ^{17}B are calculated by Eq. (18).

Figure-2 shows the dependence of the matter density distributions (in fm^{-3}), calculated via the TFSM, on r (in fm) for ^{8}He figure-2-a and ^{17}B figure-2-b exotic nuclei. The dashed, dash-dotted and solid curves are the calculated results when the valence two neutrons in ^{8}He [^{17}B] move in the pure $1p_{1/2}$ [$2s_{1/2}$] orbit, the pure $1d_{5/2}$ [$1d_{3/2}$] orbit and the model space of ZBM [HASP], respectively. The experimental matter densities of ^{8}He (denoted by the shaded area) [4] and ^{17}B (denoted by filled circle symbols) [38] are also displayed for comparison. It is clear from figure-2 that the performance of the dashed, dash-dotted and solid distributions are approximately the same throughout the entire range of

considered r. In figure-2-a, the dashed and solid distributions (coincide with each other throughout all range of r) are better describing the data than the dash-dotted one. In figure-2-b, the solid distribution is better representing the data than the others.

Figure-3 demonstrates the contributions of the core nucleons (dashed curves) and the two valence neutrons (dash-dotted curves) to the matter density (solid curves) obtained by the TFSM figure-3-a and figure-3-c and BCM figure-3-b and figure-3-d. The top and bottom panels correspond to exotic nuclei ^{8}He and ^{17}B, respectively. The feature of the long tail behavior (considered as a distinctive feature of halo nuclei) is exemplified in all solid distributions of figure-3. Hence this behavior (which is due to the two valence neutrons) is in agreement with the experimental data.

Figure-4 illustrates the calculated proton and neutron density distributions displayed as dashed and dash-dotted curves, respectively. These distributions are calculated by the TFSM figure-4-a and figure-4-c and BCM figure-4-b and figure-4-d. The long tail performance is clearly noticed in the dash-dotted curves. This performance is related to the existence of the valence two neutrons in the halo orbits. The steep slope performance is obviously observed in the dashed curves due to the absence of protons in the halo orbit, where all protons of these nuclei are found in its core only. The difference between the calculated neutron and proton rms radii is $R_n - R_p = 2.88 - 2.08 = 0.80$ fm for ^{8}He and $R_n - R_p = 3.27 - 2.15 = 1.12$ fm for ^{17}B. This difference also gives a supplementary support for the halo structure of these nuclei.

Figure-5 exhibits the comparison between the calculated matter density distribution of unstable nuclei ^{8}He and ^{17}B (solid curves) and those of stable nuclei ^{4}He and ^{10}B (dashed curves). To reproduce the experimental matter rms radius 1.57 ± 0.04 [2.56 ± 0.23] fm [37] for the stable nucleus ^{4}He [^{10}B], we utilize a value for the parameter $\beta = 1.282$ [1.767] fm. The calculated densities in figure-5-a and figure-5-c [obtained via TFSM] are compared with corresponding densities in figure-5-b and figure-5-d [obtained via BCM]. It is clear from these figures that the solid and dashed curves are diverse. As the valence two neutrons in ^{8}He [^{17}B] is weakly bounded, the solid curve has a longer tail than that of the dashed curve. Figure-4 and figure-5 provide the conclusion that the halo phenomenon in ^{8}He and ^{17}B is connected to the valence neutrons but not to the core nucleons.

Elastic electron scattering proton form factors (which are simply given as Fourier transform of the ground state proton density distributions) for unstable exotic nuclei ^{8}He and ^{17}B are calculated via the plane wave born approximation (PWBA). As the calculations in the BCM do not distinguish between protons and neutrons, the ground state proton density distributions used in the calculations of the elastic form factors are restricted only to those obtained by TFSM.

Figure-6 exemplifies the comparison between the calculated elastic proton form factors of unstable nuclei ^{8}He and ^{17}B (solid curves) and those of stable nuclei ^{4}He and ^{10}B (dashed curves). Figure-6-a and figure-6-b demonstrate the proton form factors for nuclei pairs (^{8}He, ^{4}He) and (^{17}B, ^{10}B), respectively. It is well known that the proton form factor is independent on detailed properties of the two valence neutrons. The major difference between the calculated form factors of unstable nuclei (^{8}He and ^{17}B) and those of stable nuclei (^{4}He and ^{10}B) is the difference in the center of mass correction which depends on the mass number and the size parameter β which is assumed in this case equal to the average of β_c and β_v. It is clearly noticed that the dashed and solid curves in figure-6-a have no diffraction minimum throughout all range of momentum transfer while those in figure-6-b each has only one diffraction minimum, [located at momentum transfer $q = 1.80$ fm^{-1} (dashed curve) and 2.10 fm^{-1} (solid curve)], and one diffraction maximum, [located at $q = 2.15$ fm^{-1} (dashed curve) and 2.50 fm^{-1} (solid curve)]. The location of the minimum of the unstable ^{17}B (solid curve) has forward shift as compared with the minimum of the stable ^{10}B (dashed curve).

The reaction cross sections (σ_R) are studied by means of the Glauber model with an optical limit approximation at high energies for (^{8}He and ^{17}B) projectiles incident on the target of ^{12}C (rms = 2.31 $\pm$ 0.02 fm [37]) using the ground state densities of these nuclei. The densities of the projectile and target are described by single Gaussian functions with range parameters α_P and α_T for projectile and target nuclei, respectively. The calculated reaction cross sections are listed in table-2 along with the corresponding experimental data taken from [37]. The calculated σ_R at 790 MeV for ^{8}He + ^{12}C system is 863 mb, which agrees reasonably with the analogous measured data 817±6 mb [37]. The

calculated σ_R at 790 MeV for ^{17}B + ^{12}C system is 1193 mb, which agrees with the corresponding experimental data 1150±200 mb within quoted error [37].

Table 2- Calculated reaction cross sections for ^{8}He and ^{17}B exotic nuclei.

Exotic Nuclei	Experimental rms radii (fm)	Calculated σ_R (mb)	Experimental σ_R (mb)	Energy (MeV)
^{8}He	2.70±0.03 [2]	863	817± 6 [37]	790
^{17}B	2.99±0.09 [37]	1193	1150±200 [37]	790

Summary and conclusions

The ground state proton, neutron and matter densities of exotic nuclei ^{8}He and ^{17}B are studied by means of the TFSM and BCM. The long tail performance, presumed as a typical property for the halo structure, is clearly revealed in the calculated neutron and matter density distributions of these exotic nuclei. Moreover, the noticeable difference which is found between the calculated overall neutron and proton rms radii as well provides a supplementary support for the halo structure of these nuclei.

Elastic electron scattering proton form factors for these exotic nuclei are also studied using the TFSM. It is found that the major difference between the calculated form factor of unstable exotic nucleus ^{8}He [^{17}B] and that of a stable nucleus ^{4}He [^{10}B] is the difference in the center of mass correction which depends on the mass number and the size parameter β (which is assumed in this case equal to the average of β_c and β_v).

The reaction cross sections for these exotic nuclei are studied by means of the Glauber model with an optical limit approximation using the ground state densities of the projectile and target, where these densities are described by single Gaussian functions. The calculated reaction cross sections of ^{8}He and ^{17}B at high energy (790 MeV) are in agreement with those of experimental data. The analysis of the present study suggests that the structure of the two valence neutrons in ^{8}He [^{17}B] is mixed configurations with dominant $(1p_{1/2})^2$ [$(2s_{1/2})^2$]. The present study supports the halo structure of these nuclei.

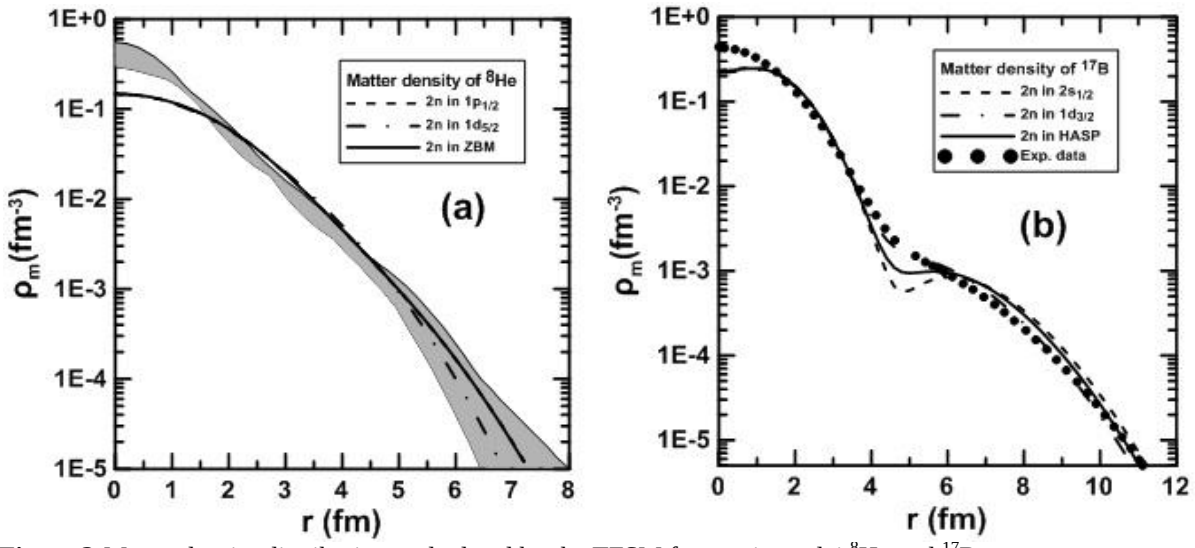

Figure.2-Matter density distributions calculated by the TFSM for exotic nuclei ^{8}He and ^{17}B.

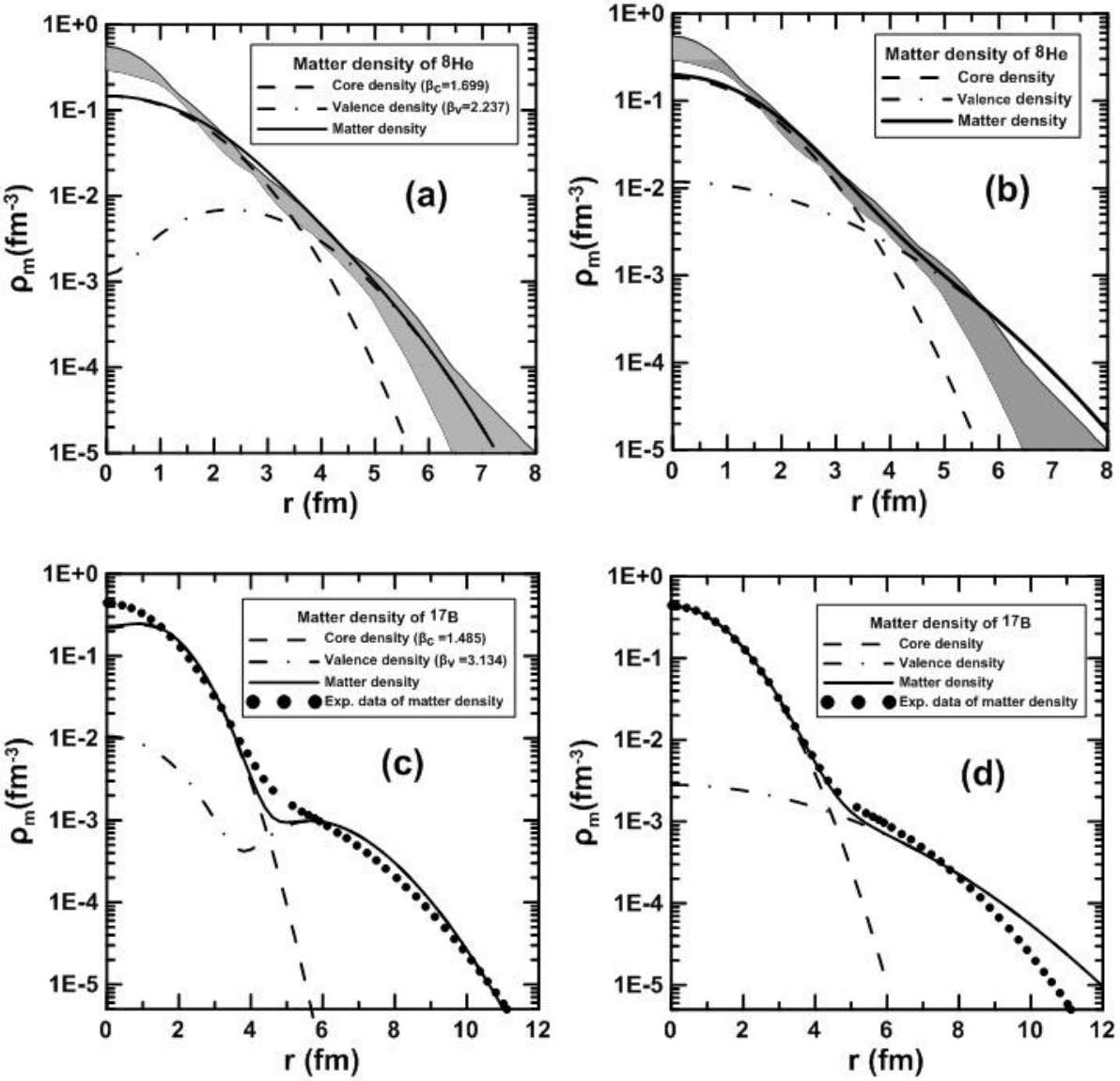

Figure.3-The calculated matter density distributions obtained via TFSM [figure a and figure c] and BCM [figure b and figure d].

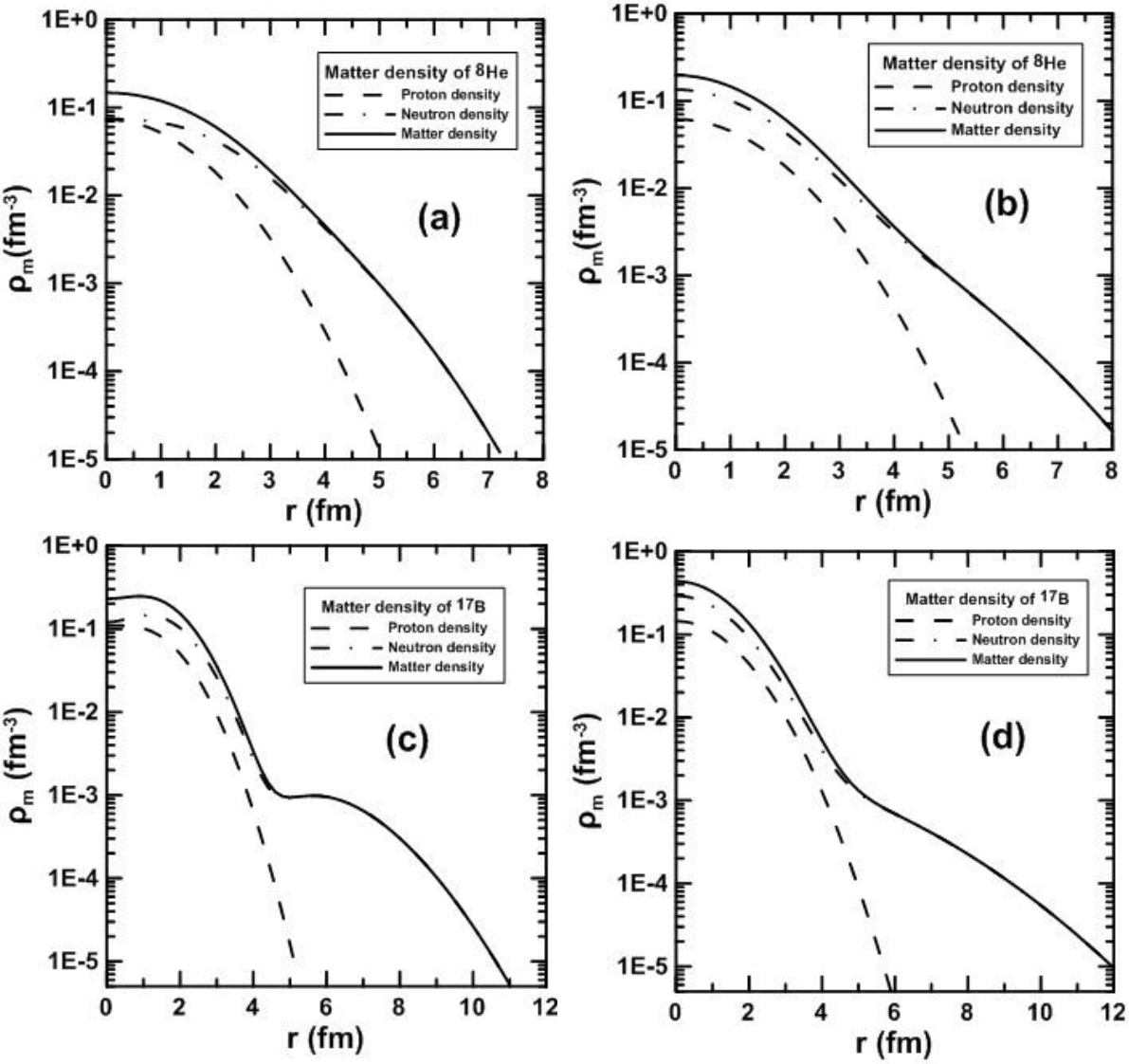

Figure.4-Neutron, proton and matter density distributions obtained via TFSM [figure a and figure c] and BCM [figure b and figure d].

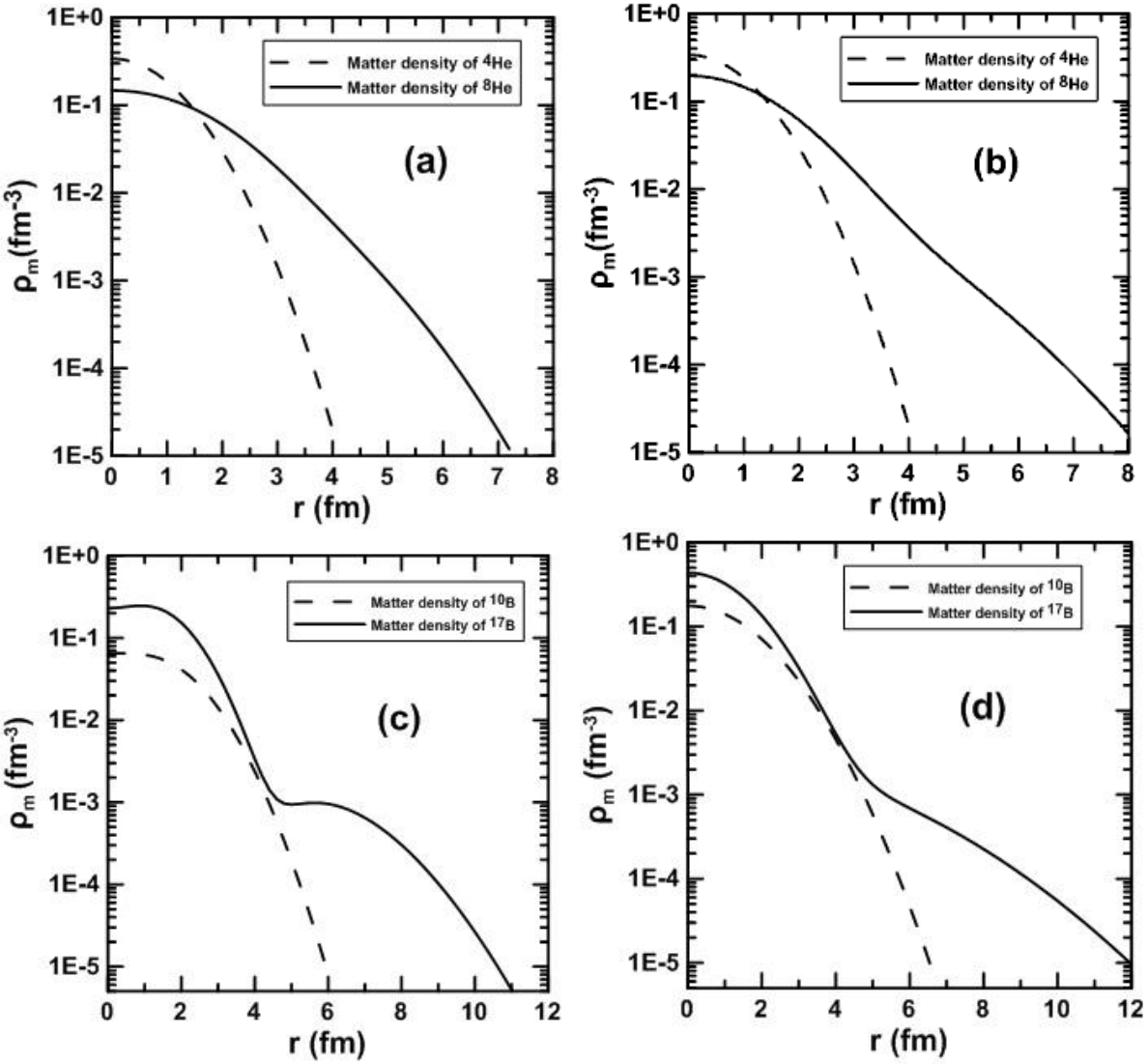

Figure.5-The comparison between the calculated matter density of unstable and stable nuclei. The left and right columns correspond to the calculations of TFSM and BCM, respectively

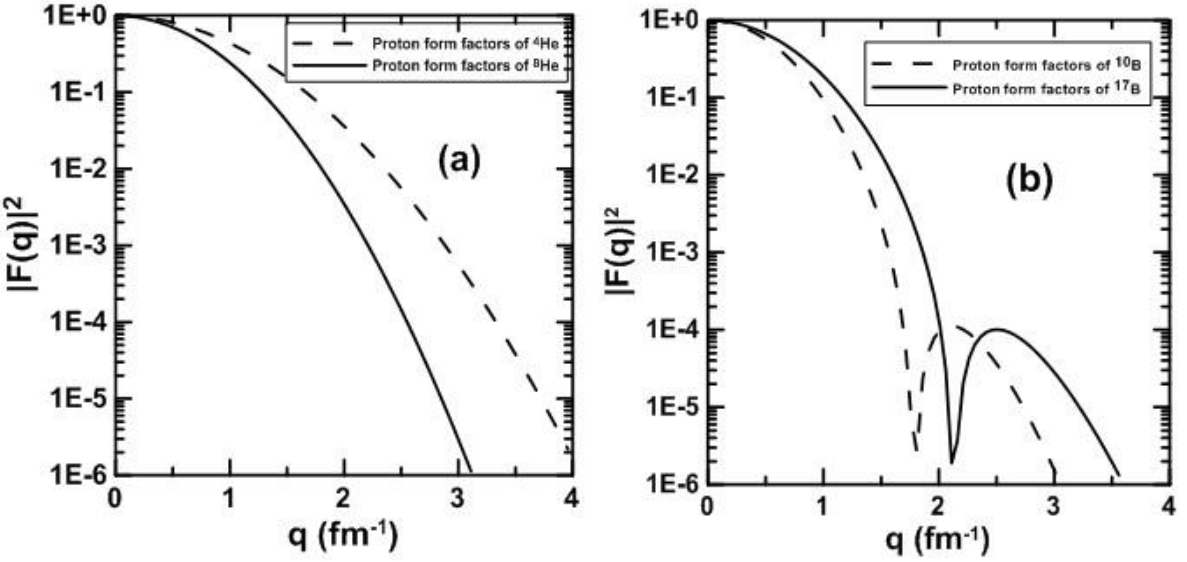

Figure.6-The comparison between the calculated proton form factors of unstable (exotic) nuclei and those of stable nuclei.

References

1. Tanihata I.,Hamagaki H.,Hashimoto O.,Nagamiya S.,Shida Y.,Yoshikawa N.,Yamakawa O.,Sugimoto K.,Kobayashi T.,Greiner D. E.,Takahashi N. and Nojiri Y. **1985.** Measurement of interaction cross sections and radii of He isotopes. *Physics Letters B*, **160**(6),pp: 380-384.
2. Tanihata I., Hamagaki H., Hashimoto O., Shida Y., Yoshikawa N., Sugimoto K., Yamakawa O, and Kobayashi T.**1985**. Measurement of interaction cross sections and nuclear radii in the light p-shell region. *Physical Review Letters*,**55** (24), pp:2676-2679.
3. Zukov M. V.,Danilin B. V.,Fedorov D. V.,Bang J. M.,Thompson I. J. and Vaagen J. S.**1993**. Bound state properties of Borromean halo nuclei: ^{6}He and ^{11}Li. *Physics Reports*. **231**(4), pp:151-199.
4. Antonov A. N., Kadrev D. N., Gaidarov M. K., Moya de Guerra E., Sarriguren P., Udias J. M., Lukyanov V. K., Zemlyanaya E. V., and Krumova G. Z. **2005**. Charge and matter distributions and form factors of light, medium, and heavy neutron-rich nuclei. *Physical Review C* **72**, pp:1-11.
5. Donnelly T. W. and Walecka J. D. **1975**. Electron scattering and nuclear structure. Annual Review of Nuclear Science **25**, pp:329- 405.
6. Technical Proposal for the Design, Construction, Commissioning, and Operation of the ELISe setup, Haik Simon, GSI Internal Report, Dec. 2005.
7. Suda T. and Wakasugi M. **2005**. Structure studies of unstable nuclei by electron scattering. Progress in Particle and Nuclear Physics. **55**, pp:417-436.
8. Alkhazov G.D., Dobrovolsky A.V. and Lobodenko A.A.. **2004**. Matter density distributions and radii of light exotic nuclei from intermediate-energy proton elastic scattering and from interaction cross sections.*Nuclear Physics* A **734** , pp:361-364.
9. Alkhazov G.D., Dobrovolsky A.V., Egelhof P., Geissel H., Irnich H., Khanzadeev A.V., Korolev G.A., Lobodenko A.A., Münzenberg G., Mutterer M., Neumaier S.R., Schwab W., Seliverstov D.M., Suzuki T., Vorobyov A.A. **2002**. Nuclear matter distributions in the ^{6}He and ^{8}He nuclei from differential cross sections for small-angle proton elastic scattering at intermediate energy. *Nuclear Physics* A **712** , pp:269-299.
10. Korsheninnikov A.A., Kuzmin E.A., Nikolskii E.Yu., Bertulani C.A., Bochkarev O.V., Fukuda S., Kobayashi T., Momota S., Novatskii B.G., Ogloblin A.A., Ozawa A., Pribora V. , Tanihata I. and Yoshida K. **1997**. Elastic and inelastic scattering of exotic nuclei. *Nuclear Physics* A **616**, pp: 189-200.
11. Korsheninnikov A.A., Nikolskii E.Yu., Bertulani C.A., Fukuda S., Kobayashi T., Kuzmin E.A., Momota S., Novatskii B.G., Ogloblin A.A., Ozawa A., Pribora V., Tanihata I. and Yoshida K. **1997.** Scattering of radioactive nuclei ^{6}He and ^{3}H by protons: Effects of neutron skin and halo in ^{6}He, ^{8}He and ^{11}Li. *Nuclear Physics* A **617**, pp:45-56.
12. Avrigeanu M., Anagnostatos G.S.,Antonov A.N. and Avrigeanu V. **2002**. Elastic scattering as a test of density distributions in ^{6}He and ^{8}He. *International Journal of Modern Physics* E **11**, pp:249.
13. Ren Z. Z. and Xu G. O. **1990**. A three-body model of $^{l\,1}$Li, ^{14}Be and ^{17}B. *Physics Letters*. B **252** (3), pp:311-313.
14. 14 – Suzuki T., Kanungo R., Bochkarev O., Chulkov L., Cortina D.,Fukuda M., Geissel H., Hellstrom M., Ivanov M., Janik R., Kimura K., Kobayashi T., Korsheninnikov A.A., Munzenberg G., Nickel F., Ogloblin A.A., Ozawa A., Pfutzner M., Pribora V., Simon H., Sitar B., Strmen P., Sumiyoshi K., Summerer K., Tanihata I., Winkler M. and Yoshida K. **1999**. Nuclear radii of ^{17,19}B and ^{14}Be. *Nucl Phys* A **658**, pp:313–326.
15. Cai X., Feng J., Shen W., Ma Y., Wang J. and YeW. **1998**. In-medium nucleon-nucleon cross section and its effect on total nuclear reaction cross section. *Physical Review C* 58, pp 572.
16. Tanihata I., Hirata D., Kobayashi T., Shirnoura S., Sugimoto K. and Toki H. **1992**. Revelation of thick neutron skins in nuclei. *Physics Letters. B* **289**, pp:261-266.
17. Tetsuaki M. **2011**. Density distributions for two neutron halo nuclei ^{11}Li and ^{14}Be deduced by the reaction cross section measurements. Ph.D.Thesis. Department of physics, College of Science, University of Tsukuba.
18. Ogawa Y., Yabanab K. and Suzuki Y. **1992**. Glauber model analysis of the fragmentation reaction cross sections of ^{11}Li. *Nuclear Physics A* 543, pp:722-750.

19. Ozawa A., Baumann T., Chulkov L., Cortina D., Datta U., Fernandez J., Geissel H., Hammache F., Itahashi K., Ivanov M., Janik R., Kato T., Kimura K., Kobayashi T., Markenroth K., Meister M., Münzenberg G., Ohtsubo T., Ohya S., Okuda T., Ogloblin A.A., Pribora V., Sekiguchi M., Sitár B., Strmen P., Sugimoto S., Sümmerer K., Suzuki T., Tanihata I. and Yamaguchi Y. **2002**. Measurements of the interaction cross sections for Ar and Cl isotopes. *Nuclear Physics A* **709**, pp:60–72.

20. Guo W. J., Jiang H. Q., Liu J. Y., Zuo W., Ren Z. Z., and Lee X. G. **2003**. Total nuclear reaction cross section induced by halo nuclei and stable nuclei. Commun. Theoretical Physics. (Beijing, China) 40 , pp:577–584

21. Tanihata I. **1996**. Neutron halo nuclei. *J. Phys. G* **22**, pp:157-198.

22. Zhao Y.L., Ma Z.Y., Chen B.Q. and Sun X.Q. **2001**. Extended Glauber theory and its application in halo nucleus scattering. High Energy Phys. *Nuclear Physics* **6**,pp:506.

23. Brown B. A., Radhi R. and Wildenthal B. H. **1983**. Electric quadrupole and hexadecupole nuclear excitations from the perspectives of electron scattering and modern shell-model theory. Physics Reports. **101**(5), pp:313-358.

24. Brown B. A., Etchegoyen A., Godwin N. S.,Rae W. D. M., Richter W. A., Ormand W.E., Warburton E. K., Winfield J. S., Zhao L., Zimmerman C. H. 2005. Oxbash for Windows PC. MSU-NSCL report number 1289.

25. Kuo T. T. S., Muether H. and Amir-Azimi-Nili K. **1996**. Realistic effective interactions for halo nuclei. *Nuclear Physics A*. **606**, pp:15-26.

26. Kuo T. T. S., Krmpotic F. and Tzeng Y. **1997**. Suppression of core polarization in halo nuclei. *Physical Review Letter* **78** (14), pp:2708-2711.

27. Tostevin J. A., Johnson R. C. and Al-Khalili J. S.**1998**. Manifestation of halo size in scattering and reactions. *Nuclear Physics A* **630**, pp:340c-351c.

28. Zheng T., Yamaguchi T., Ozawa A., Chiba M., Kanungo R., Kato T., Katori K., Morimoto K., Ohnishi T., Suda T., Tanihata I., Yamaguchi Y., Yoshida A., Yoshida K., Toki H. and Nakajima N. **2002**. Study of halo structure of ^{16}C from reaction cross section measurement. *Nuclear Physics* A **709**, pp:103-118.

29. Tostevin J. A. and Al-Khalili J. S. **1997**. How large are the halos of light nuclei. *Nuclear Physics* A **616** , pp:418c-425c.

30. Charagi S.K. and Gupta S.K. **1990**. Coulomb-modified Glauber model description of heavy-ion reaction cross sections. *Physical Review C* **41**, pp:1610-1618.

31. Audi G, Wapstra A. H. and Thibault C. **2003**. The AME 2003 atomic mass evaluation (II). Tables, graphs and references *Nuclear Physics A* 729, pp:337–676.

32. Audi G., Bersillon O., Blachot J. and Wapstra A.H. **2003.** The NUBASE evaluation of nuclear and decay properties. *Nuclear Physics **A*** 729, pp:3-128

33. McGrory J. B. and Wildenthal B. H. **1973**. Shell-model calculations for A=18, 19, and 20 nuclei with core excitation included explicity. *Physical Review C* **7**, 974.

34. Hasper H. **1979**. Large scale shell-model calculations in the upper part of the sd shell: General description and energy levels for *A*=36−39. *Physical Review C* **19**, 482.

35. Egelhof P. **2001**. Nuclear matter distributions of neutron-rich halo nuclei from intermediate energy elastic proton scattering in inverse kinematics. Progress in Particle and *Nuclear Physics* **46**, pp:307-316.

36. Wang M., Hu Z.-G., Xu H.S., Sun Z.-Y.,Wang J.S., Xiao G. Q., Zhan W. L., Zhang X. Y., Li C., Mao R. S., Zhang H. B., Zhao T. C., Xu Z. G., Wang Y., Chen R. F., Huang T. H., Gao H., Jia F., Fu F., Gao Q., Han J. L., Zhang X. H., Zheng C., Yu Y. H., Fan R. R., Li B. and Guo Z. Y. **2008**. Configuration of the valence neutrons of ^{17}B. Chinese Physics C **32** (7), pp:548 -551.

37. Ozawa A., Suzuki T., Tanihata I.**2001**. Nuclear size and related topics. *Nuclear Physics A* **693** pp:33-62.

38. Hu Z., Wang M., Xu H., Sun Z., Wang J., Xiao G., Zhan W., Xiao Z., Mao R.,2, Li C., Zhang X., Zhang H., Zhao T., Xu Z., Wang Y., Chen R., Huang T., Fu F., Gao Q., Han J., Zhang X., Zheng C., Yu Y. and Guo Z. **2008**. The properties of halo structure for ^{17}B. Science in China Series G: Physics, Mechanics & Astronomy 51 (7), pp: 781-787.